A&A 507, 1015–1022 (2009)
DOI: 10.1051/0004-6361/200912639

Astronomy & Astrophysics

Meteosat observation of the atmospheric entry of 2008 TC_3 over Sudan and the associated dust cloud

J. Borovička[1] and Z. Charvát[2]

[1] Astronomical Institute of the Academy of Sciences, Fričova 298, 25165 Ondřejov Observatory, Czech Republic
e-mail: borovic@asu.cas.cz
[2] Czech Hydrometeorological Institute, Satellite Department, Na Šabatce 17, 14306 Praha 4, Czech Republic
e-mail: zdenek.charvat@chmi.cz

Received 5 June 2009 / Accepted 23 July 2009

ABSTRACT

We analyzed serendipitous observations by the Meteosat 8 weather satellite of the fireball caused by the entry of the small asteroid (or large meteoroid) 2008 TC_3 over northern Sudan on October 7, 2008. Meteosat 8 scans the Earth in 5 min cycles. The fireball was captured in the 2:45 UT images in four visible-near infrared channels (0.6–1.6 μm) at a height of 45 km, and in eight mid infrared channels (3.9–13.4 μm) at a height of 33 km. The latter channels also detected at least two dust clouds deposited in the atmosphere at the heights of about 44 and 36 km. The dust deposition was a result of severe atmospheric fragmentation of the asteroid, accompanied by fireball flares, which could be detected in the light scattered by the Earth's surface. The fireball brightness was measured at two random heights, 45 and 37.5 km, where it reached −18.8 and −19.7 mag, respectively. The peak brightness was probably higher than −20 mag. The color temperature of the fireball at 45 km was 3650 ± 100 K. Infrared spectra of the fresh dust clouds were dominated by the 10 μm Si-O band caused by recondensed amorphous silicates. Five minutes later, the dust clouds were detected in absorption of thermal radiation of the Earth. At that time, the silicates were largely crystalline, suggesting silicate smoke temperatures exceeding 1000 K. The total mass of the silicate smoke was estimated to be 3100 ± 600 kg. More mass was probably contained in larger, micron sized, and colder dust particles resulting from incomplete sublimation of the asteroidal material and detected later by Meteosat 8 and 9 in scattered sunlight. Based on the heights of asteroid fragmentations, we guess that the bulk porosity of 2008 TC_3 was of the order of 50%, i.e. higher than the porosity of the recovered meteorite Almahata Sitta.

Key words. meteors, meteoroids – minor planets, asteroids – Earth – infrared: solar system

1. Introduction

On October 6, 2008, 6:39 UT, R. Kowalski at the Catalina Sky Survey discovered a new asteroid, later designated 2008 TC_3. After additional observations from Arizona and Australia, it became clear that it was a very small body of several meters in diameter that was heading towards the Earth. Soon after, Chesley predicted that the atmospheric entry would occur on Oct. 7, 2:46 UTC (one hour before local sunrise) over northern Sudan (Chesley 2008). There was no time to set up any scientific observation of the anticipated fireball. Indirect reports published on the internet indicated that ground illumination by the fireball was visible on a webcamera located in El Gouna, Egypt (735 km from the fireball trajectory)[1] and that the scattered fireball light was noticed by airplane pilots flying over Chad, ≈1400 km from the trajectory[2] (see also Kwok 2009). P. Brown reported that sonic waves from the fireball were registered by infrasonic arrays in Kenya[2]. Direct confirmation that the fireball occurred as predicted came from US Government satellites[3]. Only later did it become clear that there were also numerous eyewitnesses and that the dust cloud left in the atmosphere by the fireball was imaged[4] from the ground during the morning twilight (Jenniskens et al. 2009; Kwok 2009). Finally, in December, 2008, the first meteorites, named Almahata Sitta, were recovered in the Nubian desert (Jenniskens et al. 2009).

In this paper we present a detailed analysis of serendipitous observations of the fireball produced by the 2008 TC_3 atmospheric entry and the associated dust cloud by Meteosat weather satellites. We briefly reported the observations shortly after the event (Borovička & Charvát 2008) and in Jenniskens et al. (2009). The description of the instrument is given in Sect. 2. The data are described in Sect. 3. In Sect. 4 we use the data for the evaluation of the fireball trajectory, heights of major fragmentations, fireball brightness, spectral energy distribution of the fireball and dust radiation, as well as total mass and subsequent evolution of the dust. The implications of our results are discussed in Sect. 5.

2. The Meteosat satellites

Meteosat 8 and 9 are geostationary weather satellites located at 9.5 and 0.0 Eastern longitude, respectively, and operated by EUMETSAT (European Organisation for the Exploitation of Meteorological Satellites). They belong to the meteosat second generation (MSG) series. The main instrument is the Spinning Enhanced Visible and Infrared Imager (SEVIRI), a 0.51-m mirror telescope with detectors of 12 spectral channels distributed in the focal plane. Simultaneous scanning of the Earth in all channels is realized by using the satellite spin (scanning in the east-west direction) and by tilting the entry mirror after each

[1] http://home.pages.at/thie/asteroid_2008_tc3/
[2] http://www.spaceweather.com/ (Archive, October 7, 2008)
[3] http://aquarid.physics.uwo.ca/~pbrown/usaf/usg282.txt
[4] http://apod.nasa.gov/apod/ap081108.html

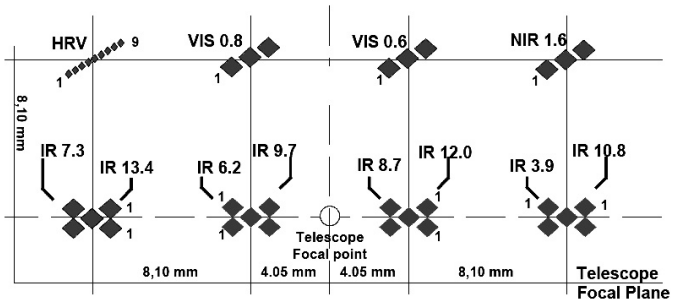

Fig. 1. Arrangement of detectors in the focal plane of the SEVIRI instrument. The separation of 8.10 mm corresponds to 54 km in the subsatellite point (adapted from EUMETSAT documentation).

Table 1. Characteristics of the spectral channels of Meteosat 8.

Channel	Central wavelength μm	$FWHM$ μm
HRV	0.67	0.43
VIS0.6	0.64	0.08
VIS0.8	0.81	0.06
NIR1.6	1.64	0.13
IR3.9	3.97	0.58
IR6.2	6.34	0.90
IR7.3	7.36	0.47
IR8.7	8.72	0.36
IR9.7	9.67	0.25
IR10.8	10.76	1.05
IR12.0	11.94	0.95
IR13.4	13.36	1.37

revolution (in the south-north direction). Since 13 May 2008, a new rapid scan service has been provided by Meteosat 8. In this regime, a restricted area (from about 15° to 70° northern latitude) is scanned every 5 min. Meteosat 9 scans the full disc in 15 min.

There are 11 narrow spectral channels with central wavelengths from 0.6 to 13.4 μm and one high resolution visible spectral channel (HRV) with wider response from 0.45 to 1.0 μm. The specifications of the channels are given in Table 1. The distribution of the detectors in the instrument focal plane is shown in Fig. 1. There are three detectors for each channel, except HRV, which has 9 detectors. At any time instant, different channels observe different parts of the Earth surface. There is a basic grid of 8.1×8.1 mm in the focal plane, which corresponds to 54×54 km on the surface (close to nadir). The detectors are diamonds with a corresponding size on one side of 4.8 km (1.6 km for HRV). During the scanning, the areas captured by the detectors partly overlap. In the final image, however, the signal received by each detector is transformed into a pixel of size 3×3 km (1×1 km for HRV).

The satellite spin period is 600 ms. During each revolution, three rows of the image (9 rows in HRV) are obtained within 30 ms (the rest of the time the instrument is pointing at empty space). The upper four channels (HRV, VIS0.6, VIS0.8, and NIR1.6; for simplicity called here visual channels) observe different rows than the rest of channels (the infrared channels). The separation of the rows is 54 km; visual channels scan more to the north. Infrared channels scan the same area as the visual channels after 6 revolutions, i.e. 3.6 s later. The time difference between neighboring channels in the same row observing the same object is only 1.44×10^{-4} s.

Table 2. Geographical coordinates of the projection of the fireball image to the Earth surface.

Channel	Longitude °E	Latitude °N
HRV	32.166	21.007
Other visual channels (average)	32.171	21.012
All infrared channels	32.36	20.93

The signal in each pixel is received as a 10-bit number. The infrared channels have been calibrated using a reference black body. In meteorological applications, the signal in each channel is normally converted into brightness temperature. For a fireball, which is much smaller than the pixel size, brightness temperature has no meaning. Nevertheless, radiation intensity in absolute units can be obtained as well. The visual channels have been calibrated indirectly using reflectance from a reference region in the Sahara.

3. Obtained data

The 2008 TC_3 fireball appeared as a bright spot over northern Sudan in all 12 channels of the 2:45 UT image of Meteosat 8. There was no cloud cover over that region and images taken at 2:40 UT show just thermal radiation of the surface. In Fig. 2, difference images (2:45 minus 2:40 UT) are presented. The fireball is point-like in the visual channels, except for the high resolution (HRV) channel, where slight elongation is apparent. The infrared channels show a more elongated object, which is, moreover, shifted to the southeast relative to the visual channels. The apparent fireball coordinates, i.e. coordinates of the projection of the fireball as seen from Meteosat 8 to the surface, are given in Table 2. Mass centers of the fireball images (using 3×3 pixels) were computed for the visual channels. For the more complex infrared images, just the coordinates of the brightest pixel are given. The pixel size in this region is 3.5×3.5 km (1.1×1.2 km in the HRV channel). At the time of observation, the satellite was located at longitude $9\overset{\circ}{.}39$ E, latitude $0\overset{\circ}{.}47$ N and altitude 35 790 km.

The difference of coordinates between visual and infrared channels is caused by the fact that both sets of channels captured the fireball at different times. The fireball was first observed by the visual channels. The absolute time of the observation is difficult to determine precisely; we were able to restrict it to $2^{\mathrm{h}}45\overset{\mathrm{m}}{.}8 \pm 0\overset{\mathrm{m}}{.}1$ UT. At that time, the infrared channels were scanning the area further south. They captured the fireball 3.0 s later, after the fireball moved by three rows of the image (corresponding to one satellite revolution) to the south and further to the east.

We also inspected the images taken at later times. Evidence of the dust cloud persisting in the atmosphere after the fireball disappeared was found as absorption features in 4 infrared channels of both satellites. The cloud absorbed the thermal radiation of the Earth. It was detectable at least until 3:35 UT in the Meteosat 8 IR10.8 channel (Fig. 3). The time sequence showed that the cloud originated in the brightest region of the infrared images taken at 2:45 UT, moved to the southwest and then gradually dispersed.

After the dust became illuminated by the Sun, it was imaged in the visual channels (including NIR1.6) of both Meteosat 8 and Meteosat 9. The first sign of the cloud appeared on the Meteosat 8 image taken at 3:20.7 UT in the VIS0.8 channel only. The best visibility was attained at about 3:35 UT, when the

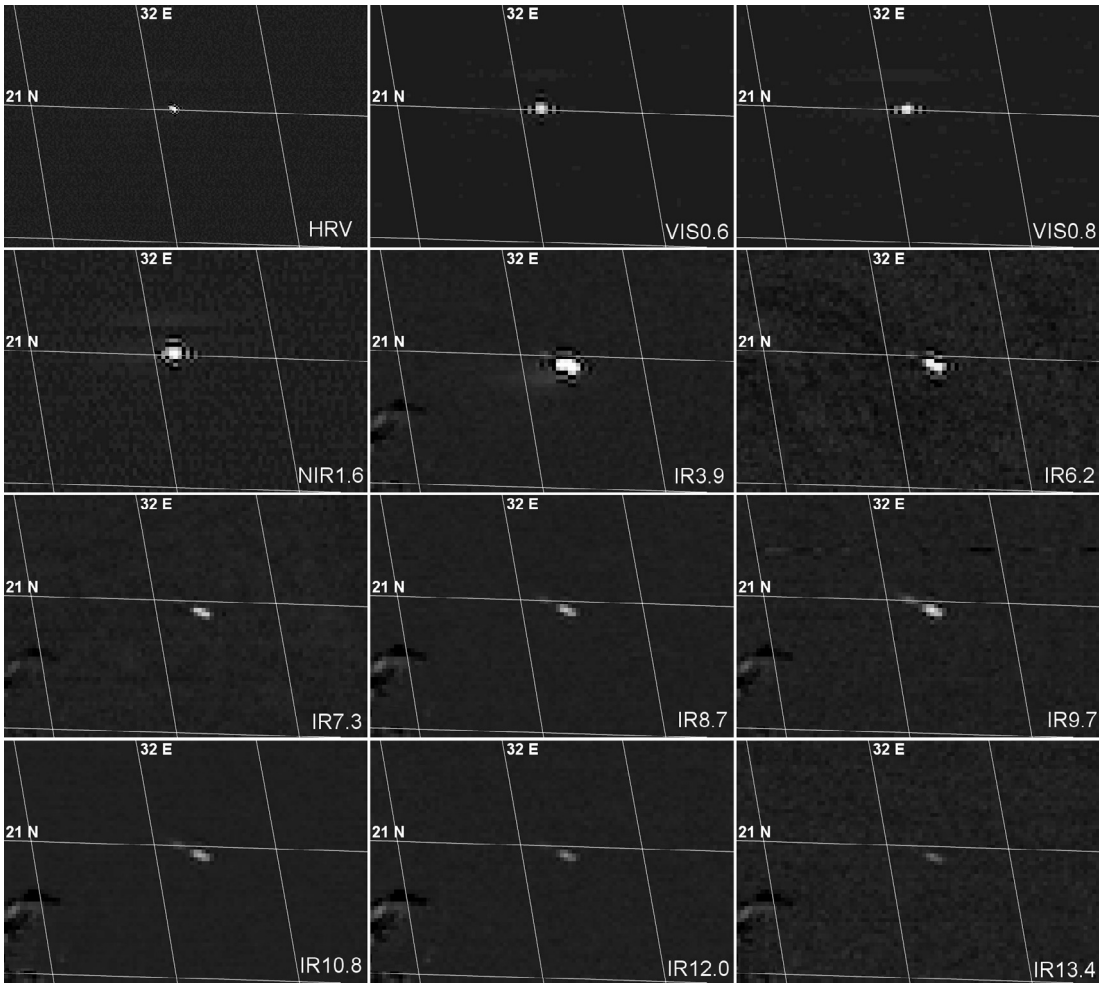

Fig. 2. Sections of Meteosat 8 images in all 12 channels taken at 2:45 UT on October 7, 2008, with the images taken 5 min earlier subtracted. Dark pixels around bright objects are artifacts of image processing. The Earth coordinate system grid is shown at an interval of one degree.

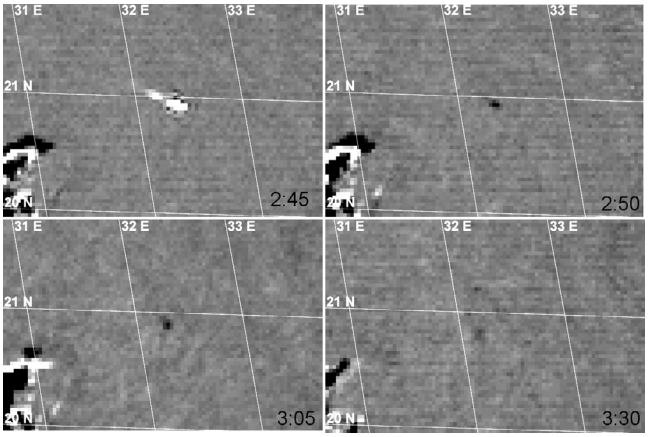

Fig. 3. Sections of Meteosat 8 images in the IR10.8 channel taken at the indicated times on October 7, 2008, with background subtracted. The background was obtained by interpolation between 2:35 UT and 3:50 UT because background intensity changed due to cooling of the Earth's surface. Brightness and contrast were enhanced. The fireball dust cloud is seen in absorption after 2:45 UT. At the lower left corner are cirrus clouds.

cloud appeared as an extended object of irregular shape (Fig. 4). There is a shift in apparent coordinates from the two satellites, which was caused by different parallax. The cloud ceased to be visible after 4:10 UT when the background became too bright. The southwestern motion persisted until that time.

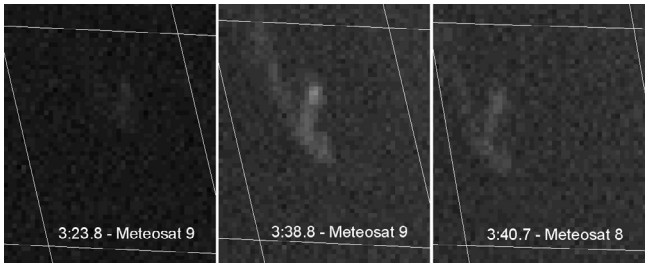

Fig. 4. Sections of Meteosat 8 and Meteosat 9 images in the HRV channel showing the fireball dust cloud illuminated by the rising Sun. The quoted times indicate the time of scanning of the displayed area. The coordinate grid is for 32°.0 and 32°.5 E and 20°.5 and 21°.0 N.

4. Analysis and interpretation

4.1. Fireball trajectory

Meteosat data do not contain full information on the fireball trajectory since the fireball was imaged from one satellite only. Nevertheless, we can compare Meteosat data with the impact trajectory computed from astrometric observations of 2008 TC_3 (Chesley et al. 2008; Jenniskens et al. 2009). According to that

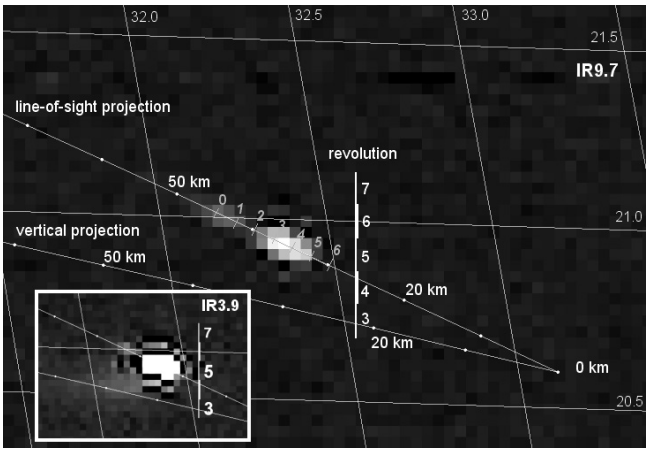

Fig. 5. Section of Meteosat 8 IR9.7 image at 2:45 UT with the 2:40 UT image subtracted. The predicted trajectory of 2008 TC_3 (Chesley et al. 2008) is shown in both vertical projection to the ground and in projection from Meteosat 8. Dots mark the meteoroid height in 10 km intervals. The rows scanned during satellite revolutions 3 to 7 are marked. The revolutions were numbered from revolution 0 corresponding to fireball capture in visual channels. Three rows of images were obtained during each revolution. The anticipated positions of the fireball at each revolution are marked on the projected trajectory. The positions were computed using the observed position in visual channels and assuming a constant fireball velocity of 12.4 km s^{-1}. The inset contains the image in the IR3.9 channel.

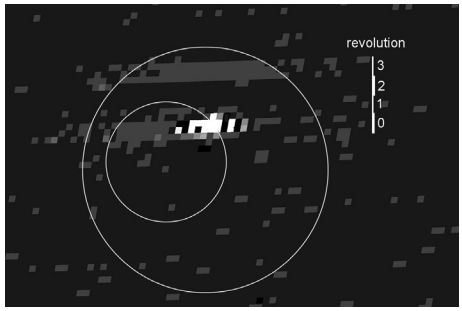

Fig. 6. Small section of Meteosat 8 VIS0.8 image at 2:45 UT with highly enhanced contrast. The rows scanned during satellite revolutions 0 to 3 are marked. Continuous bands of enhanced signal are located to the west and to the north of the fireball image and are interpreted as light from two fireball flares scattered by the ground. Two circles were drawn on the image so that they encompass each band and are centered below the position of the fireball at the time when the band was scanned. The smaller circle has a radius of 32 km (measured on the surface) and is centered below the fireball when it was at height 45 km (note that the fireball image scanned at the same time was shifted by the parallax and overlaps partly with the reflection band). The larger circle has a radius of 65 km and is centered below the fireball when it was at a height of 37.5 km. The VIS0.6 image is similar although the bands are somewhat fainter.

computation, the asteroid was located 50 km above the ground position of 31°.8038 East and 20°.8579 North at 2:45:42 UT, and was heading to ESE (azimuth 101°.6) with a descending angle of 20°.0 to the horizontal and speed of 12.4 km s^{-1} relative to the ground. The uncertainty of the position was several hundreds of meters.

Figure 5 shows the computed trajectory directly projected from the Meteosat 8 position onto the IR9.7 image. Since the satellite was located above the southwestern horizon (azimuth 230°, elevation 55°) as seen from the impact area, the projected trajectory lies apparently to the northeast of the true trajectory. The agreement of observation and computation is excellent. The IR9.7 channel shows an elongated fireball trail and the computed trajectory is projected directly onto it. Lines drawn from the points in Table 2 to the Meteosat 8 position miss the computed trajectory by less than 1 km, which is better than the precision of the observations. We can therefore consider the computed trajectory of Chesley et al. (2008) as confirmed. Meteosat data bring additional information on fireball behavior at different heights.

4.2. Heights of fireball flares

The fireball position in visual channels corresponds to the fireball at a height of 45 km. The infrared images are more complex. The signal extends over more than three rows, indicating that it was obtained during more than one scan. We numbered the satellite revolutions starting from zero for the revolution that captured the fireball in visual channels. The expected positions of the fireball at each revolution (at the time when the fireball region was scanned) are marked in Fig. 5 on the projected trajectory. It follows that infrared channels were expected to capture the fireball at revolution 5. The brightest signal was indeed obtained at that revolution. However, the brightest pixel does not correspond to the expected position of the fireball. Three seconds after passing height 45 km (±0.2 km), the fireball was expected at a height of 32.6 ± 0.3 km, assuming a realistic (small) atmospheric deceleration. The brightest pixel corresponds to the height 35.7 ± 0.7 km. Nevertheless, the pixel containing the expected fireball position is not dark and contains considerable signal in all channels. We therefore conclude that the fireball was present, but the brightest object at that time, at least at infrared wavelengths, was a dust cloud left near the position of an earlier meteoroid explosion.

A meteoroid explosion approximately at the height of 37 km was reported by US Government satellites (Jenniskens et al. 2009). Our data also contain direct evidence of the explosion. Channel IR3.9 recorded obvious diffuse signal to the left of the fireball image peaking at revolution 4 (see the inset in Fig. 5). We interpret this signal as a scattering of fireball light from the Earth's surface. Although the albedo of the surface is generally low in infrared channels, IR3.9 is an exception; the albedo in the region of interest was measured to be 24–29% in that channel.

Detailed inspection of visual channels revealed that the fireball light scattered by the surface was detected there as well, namely during revolution 3. It manifests as a 3-pixel wide horizontal band to the north of the fireball, with intensity just above the background level (Fig. 6). From the above evidence we conclude that the explosion occurred between revolutions 3–4. In visual channels, the fireball was brighter at revolution 3, when it was at height 37.5 km, while in the IR channels the illumination was higher at revolution 4, when the fireball was at 35 km. Most of the infrared illumination therefore came from the latter phase of the explosion, when a large amount of hot dust formed. The dust cloud was directly imaged in infrared channels at revolution 5 at a height of 35.7 ± 0.7 km.

Infrared channels around 10 μm revealed further dust deposition at heights of 42–45 km (Fig. 5). By chance, this cloud coincides with the position of the fireball in visual channels. Visual channels therefore captured the fireball at a phase of partial fragmentation and release of dust. The fact that the fireball experienced a flare at that time is confirmed by another scattering band recorded in visual channels at revolution 0, just to the west of the fireball image (Fig. 6). There is no scattered light in IR channels at revolution 0, but IR channels scanned an area relatively far to the south at that time.

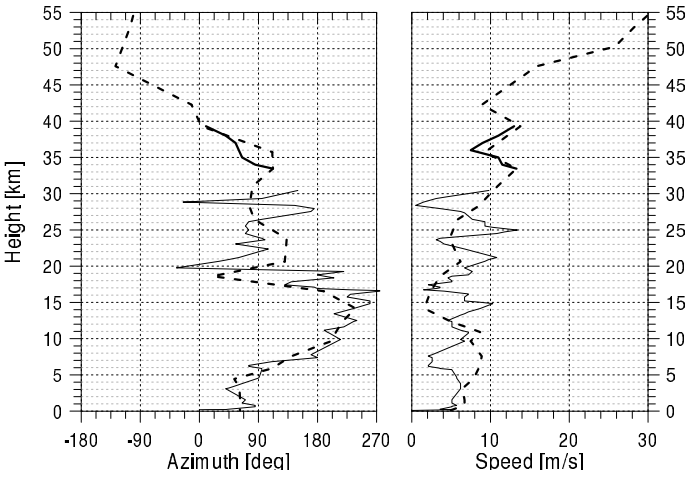

Fig. 7. Vertical profiles of wind direction (*left*) and speed (*right*) according to two sources. The thin solid line represents the radiosonde data from Asswan, Egypt (23.°96 N, 32.°77 E) taken at 0 UT, October 7 (source: University of Wyoming, http://weather.uwyo.edu/upperair/sounding.html). These data terminate at a height of 30 km. The thick dashed line is from UK Met Office wind model for coordinates 20.°81 N, 32.°34 E and October 7, 12 UT (UK Meteorological Office 2008). The thick solid line at heights around 35 km is our modification of the wind profile needed to reach agreement with the observed position of the dust cloud at 3:38.8 UT (see the text).

Another possible but uncertain dust cloud lies at a height of 53 km. A sign of it is seen only in the IR9.7 channel.

The heights of the dust clouds could be also restricted independently by using triangulation from Meteosat 8 and 9 HRV channels. We first interpolated the cloud position from two Meteosat 8 images to obtain the predicted Meteosat 8 position at 3:38.8 UT, when the Meteosat 9 image was taken (Fig. 4). The difference of apparent cloud coordinates as seen from both satellites was then measured for different parts of the cloud. The mean difference was 0.°1. The derived cloud heights range from 33 km for the northern part of the cloud to 38 km for the southern part. The brightest spot to the east was found to lie at 36±1 km, in good agreement with the height of the brightest pixel at 2:45 UT.

To further check our solution, we computed the expected dust location at 3:38.8 UT using the atmospheric wind model from the UK Met Office (Fig. 7). The agreement was good for heights 33 and 38 km but not for 36 km. To reach good agreement, we had to modify the wind profile as shown in Fig. 7. We consider this modification as plausible.

Finally, the height of the cloud could also be confirmed from the time when it started to be illuminated by the rising Sun. At $3^h20.^m7$ UT (when Meteosat 8 3:20 UT image was scanned) the full solar disk was low above the ideal horizon as seen from heights around 36 km (considering atmospheric refraction). Indeed, the southern (higher) half of the cloud was barely visible only in the VIS0.8 channel. This observation is consistent with very low elevation of the Sun and solar rays being dimmed and reddened by the passage through the troposphere.

4.3. Fireball brightness

The most straightforward way to estimate fireball magnitude is to compare the scattering of the fireball light by the ground with the scattering of solar radiation. We used channel VIS0.6 which is closest to the visual passband. The signal in the scattering bands was only 1 ADU unit above the background (dark current). We assumed the signal to be 0.5 ADU (within a factor of 2) at the edges of the bands. The edges of the northern band are located 75 km from the fireball position at the time of observation (Fig. 6). We measured the signal in the same region when it was illuminated by the Sun at a similar elevation to the elevation of the fireball (≈35° above southern horizon). We also investigated the dependence on the azimuth of the Sun in obtaining the bi-directional reflectance properly. Nevertheless, variations from pixel to pixel proved to be greater. The resulting signal from the Sun was (185 ± 30) ADU. After recomputing to the standard fireball range of 100 km, the ratio of the signals is 660:1, corresponding to a difference of 7.0 mag. Since the visual magnitude of the Sun is −26.7 mag, the fireball magnitude was −19.7 ± 0.8 mag at the time of observation, i.e. at the height of 37.5 km. Note that this is not the fireball peak magnitude. We estimate that the peak occurred about 0.2 s later. Unfortunately, Meteosat sampled the fireball region only every 0.6 s.

The same computation could be made for the second scattering band. The difference is that the edge of the band was about 55 km from the fireball (32 km horizontal distance and 45 km fireball height) and the fireball was at an elevation of 55°, where the Sun provides 250 ADU. The resulting fireball magnitude at the height of 45 km is −18.7.

The fireball magnitude also can be computed directly from the fireball signal. The brightest pixel in channel VIS0.6 has a value of 420 ADU. Nevertheless, although the fireball was surely smaller than the pixel size, the signal was spread over more pixels. We counted 2×3 pixels from revolution 0, where most signal is confined, and got 1019 ADU. Using the Meteosat calibration, this corresponds to an average specific radiation intensity over the pixel area $I_{1/\lambda} = 0.024\ \mathrm{W\,m^{-2}\,sr^{-1}\,(cm^{-1})^{-1}}$ (or, equivalently, $I_\lambda = 0.58\ \mathrm{W\,m^{-2}\,sr^{-1}\,nm^{-1}}$) at 0.64 μm. The radiation flux at the standard distance $R = 100$ km was therefore

$$F_\lambda = \pi \left(\frac{r}{R}\right)^2 I_\lambda = 1.3 \times 10^{-3}\ \ \mathrm{W\,m^{-2}\,nm^{-1}}, \qquad (1)$$

where $r = 2.7$ km is the equivalent radius of a pixel (the pixel size is 4.8 × 4.8 km). Since the flux of a zero magnitude star is $3.75 \times 10^{-11}\ \mathrm{W\,m^{-2}\,nm^{-1}}$ (Cox 1999), the fireball magnitude (at a height of 45 km) was −18.9. The agreement with the estimate obtained from ground scattering is very good.

4.4. Spectral energy distribution

4.4.1. Visible and near-infrared wavelengths

The measured radiation fluxes in the VIS0.6, VIS0.8, and NIR1.6 channels, computed from the signal of 2 × 3 pixels, have been compared with Planck functions for blackbody radiation in Fig. 8. Although the central pixel of the NIR1.6 channel reached saturation level, the surrounding pixels indicate that the saturation was only slight and that the data after a small correction could be used. The measured fluxes are compatible with a black body temperature of 3650 ± 100 K and effective diameter of the radiation volume (if assumed to be spherical) of 85 ± 8 m.

From analogy with the very bright (−19.5 mag) fireball Benešov (Borovička & Spurný 1996), we can say that the spectrum was likely not a pure blackbody. The spectrum of Benešov at maximum light contained bright continuum with superimposed emission lines. Nevertheless, unless the number of emission lines was dramatically different in different channels, the observed spectral energy distribution can characterize the temperature of the radiating region well. Previous analyses of fireball spectra (Borovička 1993; Borovička & Spurný 1996)

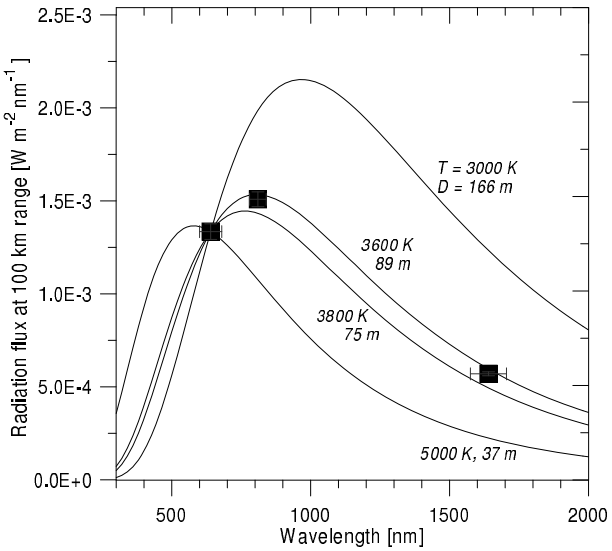

Fig. 8. Measured radiation fluxes in VIS0.6, VIS0.8, and NIR1.6 channels (squares) compared with Planck functions for T = 3000, 3600, 3800, and 5000 K. The horizontal error bars give the $FWHM$ of the channels. Vertical error bars are smaller than the symbol size. The Planck functions were scaled to match the radiation in the VIS0.6 channel. The corresponding source diameters (D) are given.

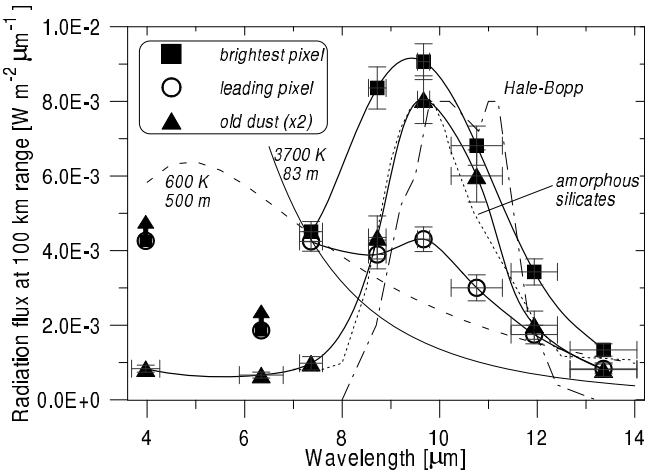

Fig. 9. Measured radiation fluxes in the infrared channels for the brightest pixel (squares), the leading pixel containing the fireball position (empty circles), and the old dust cloud at heights around 44 km (triangles). The signal of the old dust cloud was summed from 2×2 pixels and, for better comparison, multiplied by two. The horizontal error bars give the $FWHM$ of the channels. The brightest pixel and the leading pixel were both saturated in the IR3.9 and IR6.2 channels and only a lower limit of the flux could be determined at these wavelengths. Planck functions for T = 3700 K and 600 K, scaled to match the radiation in the IR7.3 channel, are plotted for comparison. Schematic shapes of the Si-O emission band in the spectrum of comet Hale-Bopp (dash-dotted line; Hanner et al. 1999) and the laboratory spectra of laser ablated amorphous olivine and enstatite summed together (dotted line; Stephens & Rusell 1979) are plotted as well.

showed that the intensities of most spectral lines can be described by a single temperature in the range 3500–5200 K. It is the temperature of the radiating gas surrounding the meteoroid and maintained at near thermal equilibrium by collisions of atoms and electrons. The temperature of the 2008 TC_3 fireball was near the lower limit of the previously observed range, probably because of low entry velocity.

The diameter of the radiation volume of 85 m is a lower limit assuming blackbody radiation. If the radiation was not optically thick at all wavelengths, the volume must have been larger to produce the observed luminosity. On the other hand, the volume was likely not spherical but elongated along the path. The high resolution HRV image (Fig. 2) suggests that the fireball was several km long at the time of observation. Nevertheless, most of the luminosity was contained at the front, where the HRV image was saturated.

4.4.2. Mid-infrared wavelengths

The image of the fireball in infrared channels is more complex than in visual channels (see Sect. 4.1). We therefore constructed three separate spectra, one for the brightest pixel, one for the leading (easternmost) pixel, containing the expected position of the fireball, and one for the separate cloud at the heights around 44 km. For that cloud, four pixels containing significant signal in all channels were summed. The 2:40 UT image was subtracted from the 2:45 UT image before counting the signal.

The resulting spectra are different from each other and are shown in Fig. 9. The spectrum of the 44 km cloud contains a single broad peak between 8–12 μm. This is evidently the 10 μm emission feature due to stretching vibrations in Si-O bonds in small (submicron) silicate grains, which was observed e.g. in the spectra of comets (Hanner & Bradley 2004). In comets, however, the band contains two peaks, at 10.0 μm and 11.2 μm. The 11.2 μm peak, attributed to crystalline olivine, is missing in our spectra. On the other hand, if compared with the laboratory spectra of laser ablated and recondensed amorphous olivine and enstatite (Stephens & Rusell 1979), the match is very good (see Fig. 9). The profiles of olivine and enstatite from Stephens & Rusell (1979) were combined in a 1:1 ratio.

The dust cloud at 44 km was observed when it was about 3 s old. We conclude that at that time, the dust mid-IR radiation was produced almost exclusively by the Si-O vibration band of recondensed amorphous olivine and pyroxene smoke. The presence of a small fraction of crystalline silicates is possible, because the emission at 10.8 μm was slightly higher than for the purely amorphous profile. Since no significant blackbody thermal emission was detected, the size of the smoke particles must have been much lower than the wavelength.

In contrast, the spectrum of the leading pixel contains only a hint of the 10 μm emission band. Most of the radiation, especially at lower wavelengths, was due to other source(s). Since we expect that pixel to contain the fireball, the contribution of the hot gas should be significant. In fact, the intensity at 7.3 μm can be explained by 3700 K blackbody radiation of a source of 83 m equivalent diameter, i.e. by the same parameters as for the fireball at a height of 45 km (derived from visual channels). Therefore we cannot exclude that the fireball reached a visual magnitude of about −19 again at the height of 32.7 ± 0.7 km. However, this is an upper limit of brightness, because part of the intensity at 7.3 μm was surely produced by another source such as thermal radiation of larger dust particles. Such a source is needed to explain intensities at $\lambda \geq 12$ μm.

Finally, the spectrum of the brightest pixel lies between the above extremes. The 10 μm silicate band was significant but another source contributed at $\lambda < 9$ μm. Most probably, this was thermal radiation of larger dust particles.

In addition to the data presented in Fig. 9, which were derived from direct imaging during revolutions 5 and 6, we also were able to compute the radiation flux in the IR3.9 channel

at revolution 4, when IR radiation was close to maximum. We used the signal scatterred from the ground (see Fig. 5). The signal, when corrected for varying surface albedo (measured during daytime), closely followed the inverse square law with fireball range. The derived radiation flux at 100 km range is 0.078 W m^{-2} μm^{-1}.

4.5. Dust absorption at later times

At later times, the dust cloud was detected by absorption of thermal radiation of the Earth's surface in channels IR8.7 to IR12.0. We measured the amount of absorbed radiation in individual pixels taking into account gradual cooling of the Earth's surface. The absorption was relatively slight, reaching maximally 3.4% per pixel in the IR10.8 channel and 1.9% per pixel in IR9.7 at 2:50 UT.

The fact that the absorption was greater in IR10.8 is surprising, because the emission at 2:45 UT was greater in IR9.7. After summing over pixels that contained noticeable absorption, the absorption was found to be 1.3× higher in IR10.8 than in IR9.7 at 2:50 UT and 1.7× higher at 2:55 and 3:00 UT. The probable explanation is that the amount of crystalline dust significantly increased during the first 5 min after the fireball. The narrow IR9.7 channel contains the 9.8 μm peak of amorphous Mg silicates (Day 1976) but falls outside the 10.0 μm peak of crystalline olivine (Day 1975). On the other hand, the IR10.8 channel contains the second (and larger) peak of crystalline olivine at 11.1 μm. Using the measurements of Day (1975, 1976), we estimated the mean mass absorption coefficients of crystalline olivine to be 300 m^2 kg^{-1} in IR9.7 channel and 600 m^2 kg^{-1} in IR10.8. For amorphous Mg silicates the coefficients are about 250 and 150 m^2 kg^{-1} in IR9.7 and IR10.8, respectively. The observed IR10.8/IR9.7 absorption ratio of 1.3 is consistent with about a 50:50 proportion of amorphous and crystalline phase, giving the combined mass absorption coefficients, κ, of 275 m^2 kg^{-1} in IR9.7 and 375 m^2 kg^{-1} in IR10.8.

Alternatively, we can say that the silicate evolution index of Hallenbeck et al. (2000) reached values greater than about 10 after 5 min. This corresponds to annealing temperatures of >1080 K in their experiments. Brucato et al. (1999), on the other hand, obtained crystalline features from initially amorphous enstatite after 7 min of annealing at 1000 K only. In the fireball cloud, the temperature of the dust certainly decreased over time. Nevertheless, from the fact that the dust was mostly amorphous a few seconds after the formation and significantly crystallized 5 min later, we can say that the dust temperature was higher than 1000 K for at least a fraction of a min.

4.6. Mass of the dust

Using the mass absorption coefficient obtained in Sect. 4.5, we can estimate roughly the total mass of dust responsible for the absorption. The average absorption over 10 pixels in the IR10.8 channel at 2:50 UT was 1.3 ± 0.2%, i.e. the average optical depth of the dust was $\tau = 0.013 \pm 0.002$. The combined area of 10 pixels is $S = 90$ km^2 (taking into account overlapping of the pixels). The mass of the dust was therefore $M = S\tau/\kappa = 3,100 \pm 600$ kg (using $\kappa = 375 \pm 50$ m^2 kg^{-1}). This estimate assumes that the dust was optically thin. If a dense optically thick dust cloud was responsible for the absorption, the total dust amount could be larger. For example, if the 3.4% absorption in one of the pixels was due to total obscuring of 3.4% of the pixel area (i.e. 0.78 km^2), the mass of the cloud was $M = \tau \times 2000$ kg, with τ unknown but much larger than unity.

The above estimate applies to the silicate smoke, i.e. particles much smaller than a micron, which effectively absorb in the Si-O band. However, the effective scattering of sunlight (up to the wavelength of 1.6 μm) by the dust after the cloud became illuminated demonstrates that particles of sizes comparable to or larger than the wavelength were present as well. They may represent remnants of particles released during meteoroid fragmentation and not completely ablated (decelerated before being ablated). Thermal radiation of such particles is probably responsible for the radiation of the fresh dust outside the 10 μm silicate band. The total mass of the particles is, however, difficult to estimate because the temperature, size distribution, and spatial distribution of the particles is unknown. Taking a temperature of 600 K, which is nearly consistent with the flux from the brightest pixel at 13.4 and 7.3 μm, and with the lower limit at 3.9 μm (see Fig. 9), counting all observed signals in the IR7.3 channel (not only the brightest pixel), and assuming a particle diameter of 1 μm, density 3000 kg m^{-3}, and no shielding, we arrived at about 10 000 kg. A higher temperature would result in lower mass, larger particles and/or partial self-shielding of particles would result in higher mass. From the fact that the dust sedimentation rate was lower than 1 km in 53 min (see Sect. 4.2), we can infer an upper limit of the particle diameter of 30 μm. Note that Klekociuk et al. (2005) observed the dust cloud created by a big fireball over Antarctica by lidar and concluded that most particles in the cloud were of micron size.

5. Discussion

The observation presented here represents the first observation of a fireball by Meteosat weather satellites. In principle, much fainter fireballs of magnitude −14 could produce a detectable signal (10 ADU units) in Meteosat night time images. The scanning mode, however, means that there is only 1:300 chance of capturing fireballs brighter than −14 mag for 1 s. Nevertheless, we recently found that Meteosat 8 captured another fireball, which occurred over northern Poland on May 31, 2009, 20:48:42 UT. It was detected in HRV, VIS0.6 and VIS0.8 channels, with the HRV signal being by far the brightest. This fact indicates that the fireball luminosity was dominated by emission lines, not thermal continuum. The HRV signal corresponds to a fireball magnitude of about −15.

The scanning mode is somewhat more favorable for detecting a fireball-produced dust cloud in infrared channels, provided that the cloud is massive enough (which was not the case of the Polish fireball).

The full discussion of our data on 2008 TC_3 should be done in synergy with other data on the asteroid, its atmospheric entry, and the recovered meteorites. Meteosat confirmed the asteroid atmospheric trajectory, which was, nevertheless, already confirmed by the recovery of the meteorites (Jenniskens et al. 2009). Meteosat further provided absolute calibration of fireball brightness at two points. Otherwise, the information on the light curve is incomplete. The light curve obtained by US Government satellites was briefly described by Jenniskens et al. (2009) but was not published. Both sources agree that the fireball was characterized by a series of flares and that the main flare occurred at a height of 37 km. Another flare was detected by Meteosat at 45–44 km. Both flares were evidently caused by meteoroid fragmentation and resulted in deposition of a large amount of dust into the atmosphere. Another flare possibly occurred at 53 km, based on signs of a dust cloud in the Meteosat IR9.7 image. An early fragmentation is confirmed by the elongated shape of the fireball at 45 km as imaged in the HRV channel. Small fragments

lagging behind the main body are an obvious explanation of the elongation (compare e.g. with the Peekskill fireball in Brown et al. 1994).

The US Government satellites detected another, and final, flare 1 s after the main flare (Jenniskens et al. 2009). This may correspond to near the time of fireball observation at 32.7 ± 0.7 km by Meteosat infrared channels. The fate of the fireball after that is uncertain. Meteosat sensors looked in other directions at later times. The fact that the fireball fell below the detection limit of US Government satellites and that no significant dust deposition was detected below 33 km either by Meteosat or by ground based dust observation (Jenniskens et al. 2009) suggests that only a small fraction of the initial mass continued the flight below 30 km. Although we cannot exclude the possibility that a relatively large body (hundreds of kg) survived all the fragmentations, there is no evidence for it and only small meteorites (≤283 g) were found (Jenniskens et al. 2009).

The multitude and relatively high altitude of fragmentation events is evidence of the fragile nature of 2008 TC_3. Different meteoroids can be best compared by the dynamic pressure, $p = \rho v^2$, acting at the moment of fragmentation. Here ρ is atmospheric density and v is meteoroid velocity. Ordinary chondrites Morávka (Borovička & Kalenda 2003) or Villalbeto de la Peña (Trigo-Rodríguez et al. 2006) fragmented most extensively under about 5 MPa. That would correspond to heights of about 25 km in the present case. As the other extreme, the series of flares of 2008 TC_3 resembles the Šumava fireball, a good example of the most fragile cometary bodies (Borovička & Spurný 1996). However, applying the same destruction depth model as for Šumava, we found that the terminal flare would be expected at 55 km, if 2008 TC_3 were a low density (≈100 kg m^{-3}) cometary body like Šumava. The best analog to 2008 TC_3 among large fireballs seems therefore to be Tagish Lake (Brown et al. 2002a). Still, 2008 TC_3 exploded a little bit higher than we would expect for Tagish Lake-like material.

Tagish Lake ungrouped carbonaceous chondrites are meteorites with the lowest known bulk density (1640 kg m^{-3}) and the highest porosity (40%). These meteorite properties are probably representative for the original Tagish Lake meteoroid (Hildebrand et al. 2006). The Almahata Sitta meteorites produced by 2008 TC_3 are rare ureilites with varying bulk densities of 2100–2500 kg m^{-3} and porosities 25–37% (Jenniskens et al. 2009). Since the atmospheric behavior suggests a lower strength of 2008 TC_3 than for Tagish Lake, we consider it possible that the bulk density of 2008 TC_3 was lower than 1700 kg m^{-3} and the bulk porosity was higher than 40%. In this view, the recovered meteorites represent the densest parts of the originally highly inhomogeneous body.

Meteosat measured the fireball color temperature of 3650 K, which is quite different from the 6000 K used in the interpretation of US Government satellite data[5]. Fortunately, because of the wide response of the satellite sensor (0.4–1.1 μm; Tagliaferri et al. 1994), the difference in the total radiative output is only 8%, changing it from 4.0×10^{11} J for 6000 K to 4.3×10^{11} J for 3650 K. The empirical relation of Brown et al. (2002b) gives a luminous efficiency of 9.3%, so that the total asteroid kinetic energy was $(4.6 \pm 0.5) \times 10^{12}$ J. If, however, the luminous efficiency was as high as 16%, as for Tagish Lake (Brown et al. 2002a), the total kinetic energy could be only 2.7×10^{12} J. The range of possible masses of 2008 TC_3 derived from the radiated energy is thus 35 000 to 65 000 kg. The preliminary volume of 2008 TC_3 from the shape model is 29 ± 6 m^3 (Scheirich et al. 2009).

Our estimate of the mass of the dust deposited in the atmosphere is in any case several times lower that the initial mass. A few thousands of kilograms recondensed as a fine silicate smoke, amorphous a few seconds after the fireball passage, but largely crystalline 5 min later. Since SiO_2, MgO, and FeO together form 90% of the mass of ureilites (Dodd 1981), silicates represent the total recondensed mass well. Rapid crystallization means that the smoke temperature was greater than 1000 K. Larger, roughly micron sized dust particles, which were never completely vaporized, were deposited in the atmosphere as well, probably in greater amounts that the smoke. Our spectra suggest that these dust particles were much colder than the smoke particles, possibly about 600 K. If they were larger than the assumed 1 μm, their mass could amount to a substantial part of the initial meteoroid mass.

Meteosat spectra represent the first infrared spectra of dust deposited in the atmosphere by a large meteoroid. Future experiments with higher temporal and spectral resolution are encouraged.

Acknowledgements. We acknowledge the use of Meteosat data provided by EUMETSAT. We thank S. Chesley for providing us the computed impact trajectory of 2008 TC_3. We thank the referee, P. Brown, for helpful comments and improvement of the language of the manuscript. The work of J.B. was supported by grant No. IAA 300030813 from GA AVČR. The institutional research plan number is AV0Z10030501.

References

Borovička, J. 1993, A&A, 279, 627
Borovička, J., & Charvát, Z. 2008, IAU Circ., 8994
Borovička, J., & Kalenda, P. 2003, Meteorit. & Planet. Sci., 38, 1023
Borovička, J., & Spurný, P. 1996, Icarus, 121, 484
Brown, P., Ceplecha, Z., Hawkes, R. L., et al. 1994, Nature, 367, 624
Brown, P. G., ReVelle, D. O., Tagliaferri, E., & Hildebrand, A. R. 2002a, Meteorit. & Planet. Sci., 37, 661
Brown, P., Spalding, R. E., ReVelle, D. O., Tagliaferri, E., & Worden, S. P. 2002b, Nature, 420, 294
Brucato, J. R., Colangeli, L., Mennella, V., Palumbo, P., & Bussoletti, E. 1999, A&A, 348, 1012
Chesley, S. 2008, Minor Planet El. Circ. 2008-T50 (issued Oct. 6, 14:59 UT)
Chesley, S., Chodas, P., & Yeomans, D. 2008, JPL Near-Earth Object Program Office Statement, Nov. 4, http://neo.jpl.nasa.gov/news/2008tc3.html
Cox, A. N. 1999, Allen's Astrophysical Quantities, 4th edn. (New York: Springer)
Day, K. L. 1975, ApJ, 199, 660
Day, K. L. 1976, ApJ, 210, 614
Dodd, R. T. 1981, Meteorites: a petrologic-chemical synthesis (Cambridge Univ. Press)
Hallenbeck, S. L., Nuth III, J. A., & Nelson, R. N. 2000, ApJ, 535, 247
Hanner, M. S., & Bradley, J. P. 2004, in Comets II, ed. M. C. Festou, H. U. Keller, & H. A. Weaver (Univ. Arizona Press), 555
Hanner, M. S., Gehrz, R. D., Harker, D. E., et al. 1999, Earth, Moon, and Planets, 79, 247
Hildebrand, A. R., McCausland, P. J. A., Brown, P. G., et al. 2006, Meteorit. & Planet. Sci., 41, 407
Jenniskens, P., Shaddad, M. H., Numan, D., et al. 2009, Nature, 458, 485
Klekociuk, A. R., Brown, P. G., Pack, D. W., et al. 2005, Nature, 436, 1132
Kwok, R. 2009, Nature, 458, 401
Scheirich, P., Ďurech, J., Pravec, P., et al. 2009, Meteorit. & Planet. Sci., in prep.
Stephens, J. R., & Rusell, R. W. 1979, ApJ, 228, 780
Tagliaferri, E., Spalding, R., Jacobs, C., Worden, S. P., & Erlich, A. 1994, in Hazards due to comets and asteroids, ed. T. Gehrels, M. S. Matthews, & A. Schumann (Univ. Arizona Press), 199
Trigo-Rodríguez, J. M., Borovička, J., Spurný, P., et al. 2006, Meteorit. & Planet. Sci., 41, 505
UK Meteorological Office [Swinbank, R., O'Neill, A., Lorenc, A.C, et al.] 2008, Stratospheric Assimilated Data, [Internet]. British Atmospheric Data Centre, Retrieved 2008 Oct. 17, Available from http://badc.nerc.ac.uk/data/assim/

[5] http://aquarid.physics.uwo.ca/~pbrown/usaf/usg282.txt